



**HAL**  
open science

## Rolls wear characterization in hot rolling process

Camille Bataille, Emilie Luc, Maxence Bigerelle, Raphaël Deltombe, Mirentxu  
Dubar

► **To cite this version:**

Camille Bataille, Emilie Luc, Maxence Bigerelle, Raphaël Deltombe, Mirentxu Dubar. Rolls wear characterization in hot rolling process. *Tribology International*, 2016, 100, pp.328-337. 10.1016/j.triboint.2016.03.012 . hal-03448196

**HAL Id: hal-03448196**

**<https://uphf.hal.science/hal-03448196>**

Submitted on 5 Apr 2024

**HAL** is a multi-disciplinary open access archive for the deposit and dissemination of scientific research documents, whether they are published or not. The documents may come from teaching and research institutions in France or abroad, or from public or private research centers.

L'archive ouverte pluridisciplinaire **HAL**, est destinée au dépôt et à la diffusion de documents scientifiques de niveau recherche, publiés ou non, émanant des établissements d'enseignement et de recherche français ou étrangers, des laboratoires publics ou privés.

# Rolls wear characterization in hot rolling process

C. Bataille <sup>a,\*</sup>, E. Luc <sup>b</sup>, M. Bigerelle <sup>a</sup>, R. Deltombe <sup>a</sup>, M. Dubar <sup>a</sup>

<sup>a</sup> Laboratoire d'Automatique, de Mécanique et d'Informatique Industrielle et Humaine, LAMIH, UMR CNRS 8201, UVHC, Le Mont Houy, 59313 Valenciennes, France

<sup>b</sup> Aludium France SAS, 82100 Castelsarrasin, France

## ARTICLE INFO

## ABSTRACT

This paper is based on the hot rolling process on stainless steels. The aim of this article is to characterize the wear of working cylinders during the hot rolling milling process. The behavior of working cylinders, used in a finishing hot rolling mill, is thus analyzed. Because of their large dimensions, the analysis of such tools cannot be carried out with usual laboratory equipment. A non-destructive methodology is proposed using replicas to measure the topography of the working cylinders. Then, two wear processes are distinguished thanks to multi-scale analysis of different roughness parameters i.e. an adhesive wear process and an abrasive wear process. A wear criterion has been defined in order to determine the maximal length of the rolling campaigns before grinding.

### Keywords:

Roughness

Wear

Rolling

High temperature

## 1. Introduction

Improving rolls' lifespan in hot rolling processes is of main concern for metal forming industries. Replacement and early breaking represent 15% of the production costs. Therefore, mastering their damage and more especially their wear becomes of major importance. The aim of the study is to characterize the evolution of the topography of the rolls in order to quantify their damage. With that aim in view, a recently developed generic method [1] is used to analyze wear during hot rolling processes. Eventually, this study will enable us to optimize the logistical organization of cylinders in order to maximize their lifetime.

## 2. Materials and methodology

### 2.1. Hot rolling mill description

Rotating rolls reduce the thickness of the material and produce long strips that can be used for manufacturing (Fig. 1). The goal of this process is to transform a slab into a thin sheet (2–4 mm) according to successive stages occurring at high temperatures, between 500 °C and 1300 °C. (Various stages compose) The hot rolling mill process is divided into different stages. At first, a slab is heated up to a temperature around 1300 °C for 3 h. At the exit of a walking beam furnace, the slab's thickness is reduced from

200 mm to 40 mm after going 5–7 times through the roughing mill. Next to this, the transfer bar is milled down into a coil of 3 mm in thickness by the finishing mill. The strip is then quenched and coiled. It takes 3 mn to roll a slab and the temperature of the transfer bar decreases from 1100 °C before the finishing mill to 950 °C after the finishing mill.

The study will focus on the finishing mill. The finishing mill is a quarto-tandem 7-stand mill which means that each stand is composed of two working rolls that are in contact with the product and two backup rolls that are used to support severe stresses by reducing deflection. In addition to this, seven stands are used for rolling. Our study will focus on the working rolls as they are in contact with the steel sheet. Thus, the surface roughness has a direct impact on the rolled steel sheet surface. A surface defect has been detected on the rolled product that was generated on finishing mill. This defect is called "rolled-in scale" defect. It has a multi-layer structure composed of alternative layers of stainless steel ductile metal and a secondary oxide layer. This defect was already studied in various articles written by Won et al. and Lee et al. [2,3,4]. These works conclude on the fact that the thin and brittle oxide layer that raises on stainless steel during hot rolling does not prevent fresh ductile metal from sticking onto working rolls. It results in a small particle of stainless steel generated onto the roll surface whose size increases after successive roll turns, estimated to 5 turns. After reaching a critical size, around 200 μm in diameter and 50 μm in thickness, the particle leaves the roll surface and can be observed on the product again. This particle will be found essentially on product edges, which will increase the planned scrap onto the affected coil. It concerns essentially ferritic alloys but can be also observed on austenitic grades. The preferential localization of the defect is

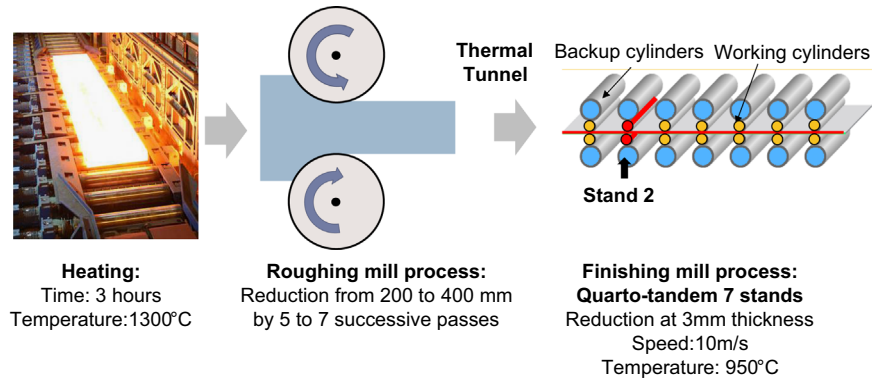


Fig. 1. Hot rolling mill process description.

explained by the same authors to be linked with product temperature. Depending on the grade, sticking temperature vary between 900 °C for low alloyed grades (such as 430) up to 1070 °C for high alloyed grades (such as 436). A second order rolling parameter pointed out in the literature is the rolling schedule (i.e. thickness reduction ratio) as described in [5]. Indeed, local high stresses will generate more fractures on the product's oxide layer, therefore generating more particles onto the working roll surface. A detailed study on the finishing mill reveals that the second stand was particularly inclined to generating "rolled-in scale" defect rather than other stands, because rolling temperatures on product edges were, for some sensitive grades, equal to the sticking temperature. Moreover, the rolling pass schedule was adapted to reduce the severity of the defect in the sense of decreasing rolling pressure on stand 2. That is why, we will investigate the wear evolution on working rolls used in the second stand with a special focus on product edges' contact areas.

This study will be focused on austenitic alloys and working rolls made of HSS (High strength steel). Consequently, working cylinders from this stand will be studied at different kilometers of rolled strips to characterize their wear. Austenitic stainless steel sheet have been studied.

## 2.2. Experimental design

In order to characterize the wear of hot rolling mill cylinders during the finishing stage, different sections of the cylinder's surface are chosen according to different process parameters as described in Table 1.

The cylinder's surface sections have been identified according to the kilometer of the cylinder, the position along the cylinder's length (11 axial positions between 00 and 20, from "the motor side" to "the operator side"), the vertical location of the working cylinders (inferior or superior), and the generatrix number (between 1 and 6). Fig. 2 shows all replicas' positions on the hot rolling milled cylinders. As a result, it enables us to analyse the evolution of roughness of rolled strip between 0 and 149 km.

## 2.3. Replication

Replicas are made on the working cylinders's surface on the 2nd stand of the finishing mill process following a defect at this step of the manufacturing process. Because of the large dimensions of the working rolls, from 680 mm to 760 mm in diameter and 2500 mm in length, some replicas are made on the surface of working cylinders. Roughness measurements are therefore readily accessible to usual laboratory measuring devices. Replicas allow us to obtain the negative of the surfaces to duplicate the surface's roughness. The Repliset T3<sup>®</sup> resin (proposed by Struers<sup>®</sup>) is used to duplicate surfaces after cleaning the cylinder with ethanol. In

Table 1

Hot rolling mill process parameters used in order to characterize wear of working cylinders.

Stainless steel type	Austenitic
Working rolls kilometers	0, 51, 88, 149 km
Working rolls location	Inferior; superior
Lateral location	From operator side to motor side in 11 positions with equidistance
Working rolls homogeneity	6 generatrix

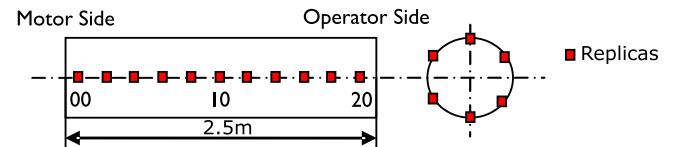


Fig. 2. Position of the replicas on hot rolling mill cylinders.

order to characterize the damage on the working cylinders' surfaces, replicas are made at different kilometers of rolled strips between two grinding operations.

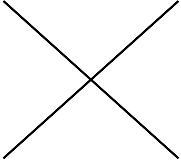
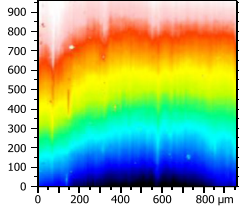
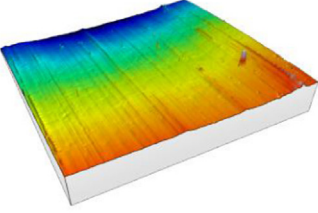
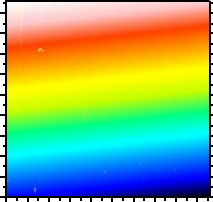
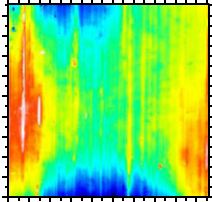
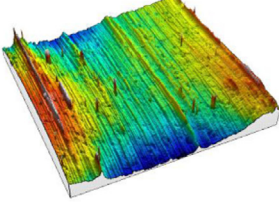
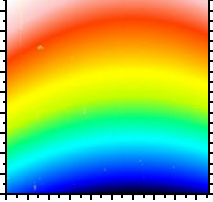
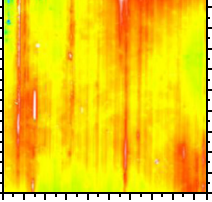
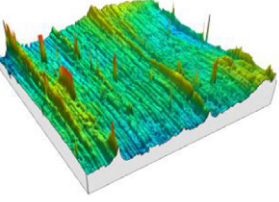
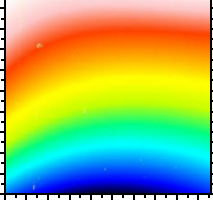
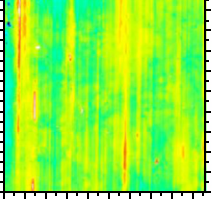
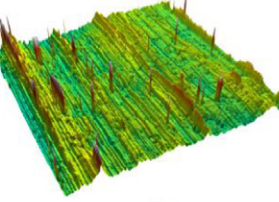
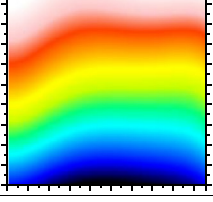
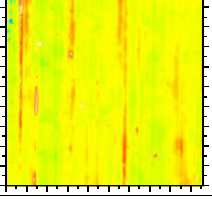
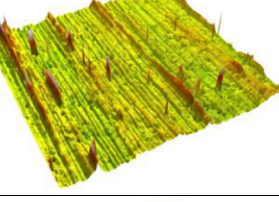
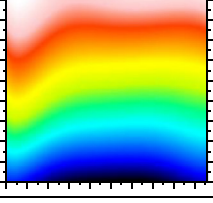
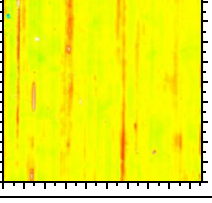
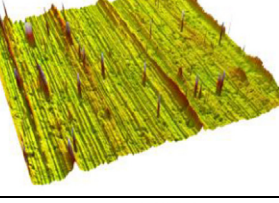
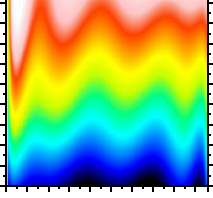
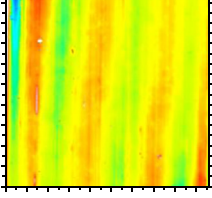
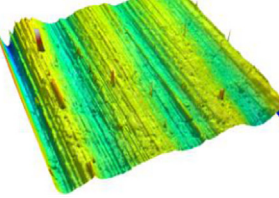
## 2.4. Roughness measurements

The white light interferometer (NewView 7300, Zygo<sup>™</sup>) is used to measure specimen topography with an  $\times 50$  Mirau objective, 0.52  $\mu\text{m}$  lateral resolution and 0.01  $\mu\text{m}$  vertical resolutions are obtained. The inspected surface area is 0.96 mm by 0.96 mm acquired by stitching on each measurement. The topographical image size is 2176  $\times$  2176 pixels. Five surfaces are randomly measured on each section of the cylinder surfaces analyzed in order to obtain robust statistic results.

## 2.5. Measurements treatment

To get reliable physical interpretation, it is very important to carry out a multi-scale analysis. Consequently, before using any filter, treatments have to be applied on all measurements. Firstly, a vertical plane symmetry perpendicular to the z axis is applied. This treatment allows us to re-establish the direction of the surface roughness altitudes. Then, a polynomial fitting is applied to remove the measured surface's form. A 3rd degree polynomial fitting is used to delete the surface form. Table 2 allows to observe surfaces after applying a polynomial treatment at different degrees. 1st and 2nd degree polynomial fittings are not adapted to the measured surfaces because they are neither flat (1st degree) nor symmetrical (2nd degree). If the polynomial degree exceeds 3, the surface's waviness might be damaged by the treatment (Table 2). When a 5 degree polynomial is applied, the waviness starts

Deleted form and surface topography at different polynomial degrees.

Polynom degree		Deleted form	2D Topography with treatment	3D Topography with treatment
0	Initial topography without treatment			
1	Ideal plan deleted <b>not appropriate</b>			
2	Symetric surfaces like (even polynom) <b>not appropriate</b>			
3	No symetric and no ideal form <b>appropriate</b>			
5	Deform the surface topography <b>not appropriate</b>			
7	Deform the surface topography <b>not appropriate</b>			
9	Deform the surface topography <b>not appropriate</b>			

being deleted and is clearly distinguished in the removed form's topography. All treatments are performed with Mesrug™ [6,7] which is software developed in our laboratory. This software

allows us to do multi-scale analysis and to determine the relevance of studied process parameters to describe some physical phenomena.

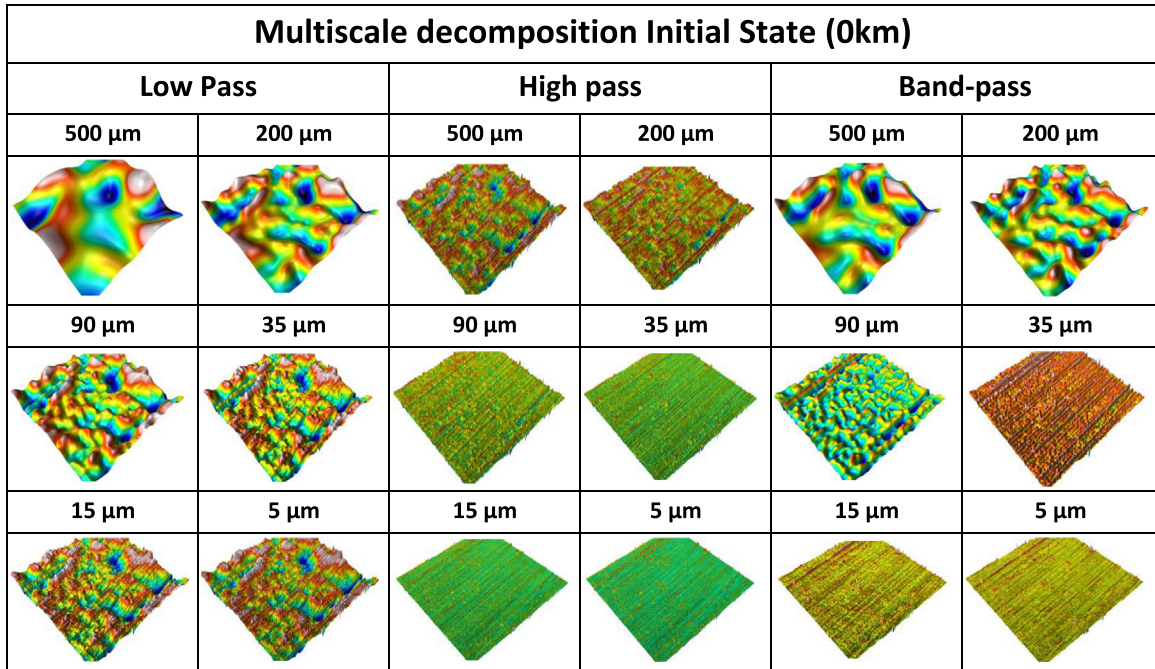


**Fig. 3.** Example of multi-scale decomposition on the initial ground cylinder using a high-pass, a low-pass and a band-pass Gaussian filter at 6 different cut-off values (500  $\mu\text{m}$ , 200  $\mu\text{m}$ , 90  $\mu\text{m}$ , 35  $\mu\text{m}$ , 15  $\mu\text{m}$ , and 5  $\mu\text{m}$ ).

## 2.6. Multi-scale decomposition

A multi-scale decomposition is processed in order to quantify the spatial scale of rolls' damage. This operation is done with Mesrug<sup>TM</sup> [6]. A Gaussian filter is used and approved by ISO 16610-2011 [8] and ASME B46.1-2009 [9]. This filter was adapted to filter the 3D surfaces with (a) given cut-off value(s). High-pass, low-pass and band-pass Gaussian filters are used with cut-off varying from 1  $\mu\text{m}$  to 223  $\mu\text{m}$ . Fig. 3 represents the decomposition of all types of Gaussian filters at 6 different cut-offs. For instance, with a high-pass Gaussian filter, when the cut-off decreases, microscopic details become visible on filtered surfaces. For each type of filter and each cut-off, 3D roughness parameters, defined by norms ISO 25178-2 [10] and EUR 15178 [11] are computed.

## 3. Results

### 3.1. Qualitative analysis of topographical maps

The topography of the initial ground cylinder is shown in Fig. 4. Upper and lower topography maps of working cylinders from the second stand of the finishing mill at 51 and 149 km are shown in Fig. 4. These maps are the most representative to observe the evolution of the hot rolling cylinder surface morphology according to kilometers. Topography maps are disposed to observe the edge of working cylinders on the left (locations: 00, 20) and the middle of working cylinders on the right (location: 10). At locations 00, 02, 18 and 20, working cylinders' surfaces are not in contact with steel sheet during the rolling process. Locations between 04 (at 480 mm from the "operator side") and 16 (at 1760 mm from the "operator side") will allow us to analyze the damage of hot rolling mill cylinders caused by the contact with the steel sheet.

We can first notice that, on the cylinder's topography maps:

1. Grooves are observed on the cylinder's surface in the same direction as the hot rolling mill direction on the entire surface of ground cylinders at 0 km (Fig. 4.1 and 4.4). They are characteristic

of grinding operations [12]. Grooves still exist at all kilometers on the edge of working cylinders (locations 00, 02, 18 and 20) as shown by Fig. 4. It is obvious because at these locations, the cylinder tips are not in contact with the steel sheet.

2. Inferior and superior cylinders, at 51 and 149 km, have symmetrical surfaces from their middle at location 10 (Fig. 4).
3. Morphology evolutions of the superior cylinder surface are observed at 51 and 149 km (Fig. 4.2 and 4.3). At 51 km, stripes and plateaus are observed on the surface between location 04 and 16 (Fig. 4.2). Largest plateaus are detected at the contact limit between the cylinder and the steel sheet (locations: 04 and 16). At 88 km, the same phenomena are noticed. At 149 km, plateaus become larger at the middle of the cylinder (Fig. 4.3) contrary to locations 04 and 16. This wear facies is associated to surface defect generation on hot rolled products. Indeed, deep grooves on cylinder surfaces are responsible for a sticking phenomenon that occurs on stainless steel products, especially because of their thin and brittle oxide layer [13,14]. At this step, the cylinder is out of order. That is the reason why the working cylinders have to be ground at this stage of wear.
4. By comparing these results to the ones corresponding to the inferior working cylinder (Fig. 4.5 and 4.6) at 51 and 149 km, a difference is noticed at 51 km (Fig. 4.5). The Largest plateaus are detected in the middle of the inferior cylinder contrary to the superior cylinder where the largest plateaus are on the product's edges. At 149 km, equivalent phenomena are observed on both cylinders (Fig. 4.6): plateaus are higher at the center of the cylinder's surfaces.

In the next part of this article, a topographical analysis is done to deduce quantitative results that will allow us to analyze deeper hot rolling mill working cylinder damage.

### 3.2. Relevance analysis of roughness parameters

Quantitative analysis is realized by multi-scale analysis to characterize the wear of working cylinders according to the corresponding scale where the phenomenon is observed. In order to

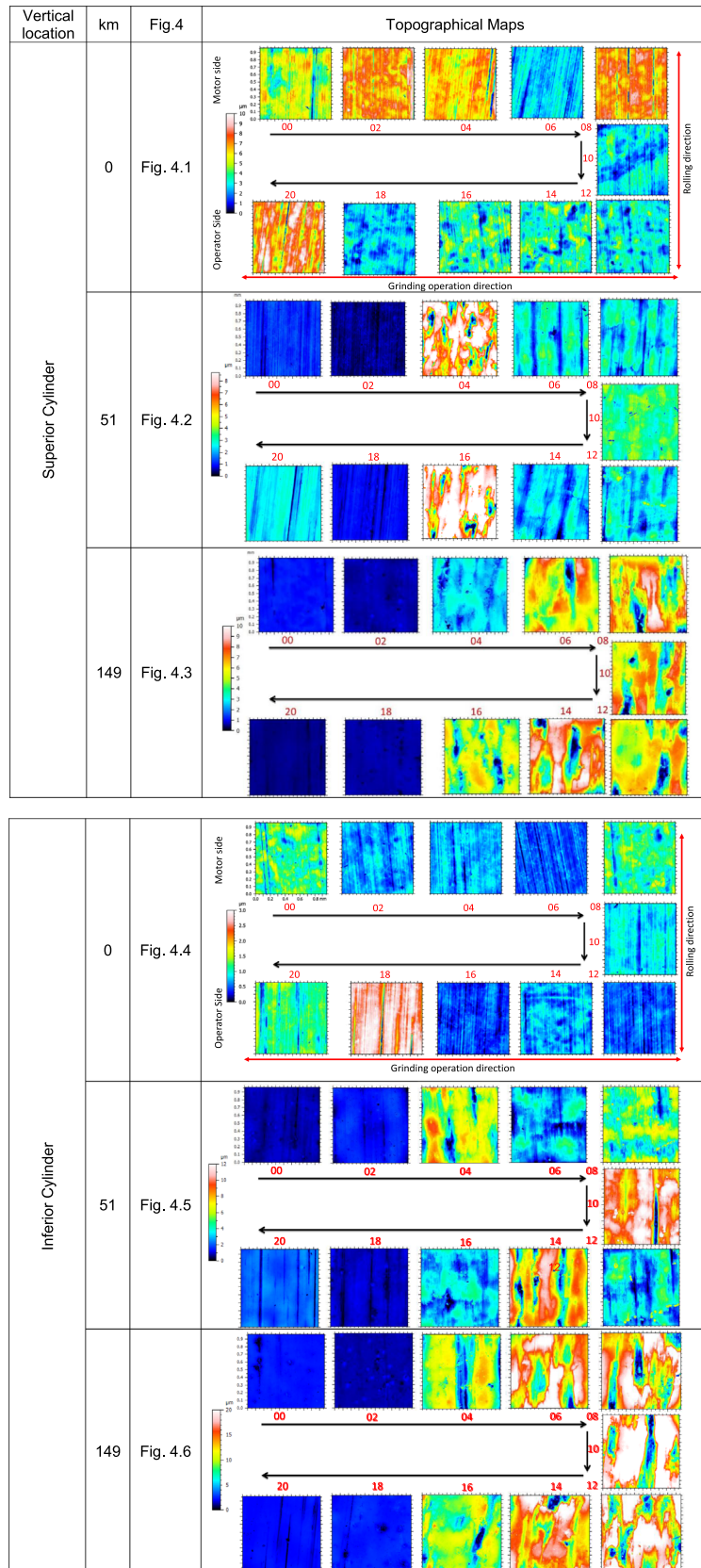


**Fig. 4.** Superior and Inferior finishing working cylinder's topography maps at 51 and 149 km. (4.1) Topography maps of the superior finishing working cylinder at 0 km, (4.2) topography maps of the superior finishing working cylinder at 51 km, (4.3) topography maps of the superior finishing working cylinder at 149 km, (4.4) topography maps of the inferior finishing working cylinder at 0 km, (4.5) topography maps of the inferior finishing working cylinder at 51 km, and (4.6) topography maps of the inferior finishing working cylinder at 149 km.

find the most representative roughness parameters of the evolution of surface topography, a multi-criteria analysis of variance (ANOVA) is applied taking into account of interactions between all selected process parameters described in the experimental design (Table 1). A bootstrap method is used to identify robust statistics [15]. The resulting value of process parameter relevance (and their interactions) is qualified by a Fisher variable ( $F$ ) affected to each roughness parameter at a set filter mode and a given cut-off. The higher the  $F$  value is, the more relevant the roughness parameter to describe the impact of the process parameter on the cylinder topography is. Therefore process parameters will be classified according to  $F$ , in decreasing order, for all roughness parameters studied and with all types of filters (5000 roughness parameters for each set of process parameter of the experimental design (Table 1). From this, plotting a relevance diagram allows us to analyze the impact of a process parameter on the cylinder morphology. The relevance diagram is achieved by using the software Mesrug™ [6]. All process parameters studied in the experimental design (Table 1) seem to influence the surface morphology. According to the diagram in Fig. 5, the mileage, the axial position (position along working cylinder's axis (from the operator side at location 00 to the motor side at location 20) and the vertical position are the most relevant process parameters. They are the best way to characterize the evolution of the cylinder surface morphology during the hot rolling mill process.

### 3.3. Multi-scale analysis

The variance analysis has shown that the  $S_a$  roughness parameter is the most relevant to characterize the cylinder damaging process after filtration with high-pass Gaussian filter.

The large amount of roughness parameters makes difficult the tribological characterization of tribofinition process like grinding, honing, lapping, coating, etc. relating to the surface function like wear, sealing, gloss, etc. The multi-scale approach, based on the relevancy of statistical methods, is used by De Chiffre et al. [17] and Berglund et al. [18]:

- De Chiffre et al. [17] used the regression coefficient according to the relative scale described in the Richardson model. This multi-scale approach allowed them to assess the strength of the thermal spray coating.
- Berglund et al. [18] used a band-pass filter to evaluate correlation between the friction coefficient and the topography of 3 dimensional surfaces. Using all ISO 25178-2 parameters, the

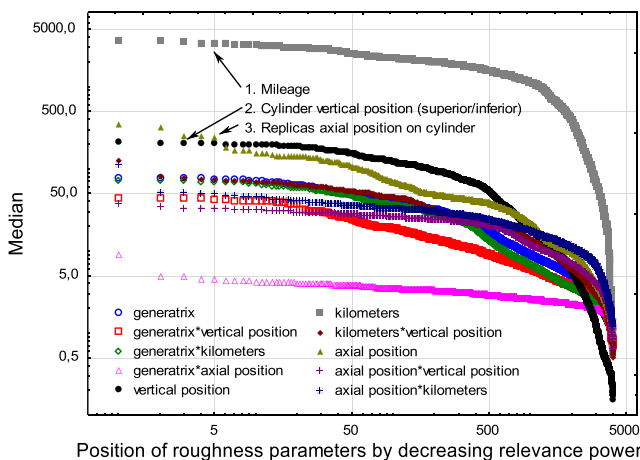


Fig. 5. Relevance diagram to analyze the impact of a process parameter on the cylinder's morphology.

multi-scale decomposition with a band-pass filter proved that  $S_a$  was the most relevant parameter at all scales.

These results demonstrate that the measuring scale does not match to the most relevant scale. Thus, surfaces have to be filtered to compute roughness parameters.

Deltombe et al., Berglund et al. and De Chiffre et al. [6,17,18] showed that only one parameter is necessary to characterize the wear on surface topography. In some cases, two parameters are needed to characterize wear mechanisms. Bigerelle et al. [7] showed that few roughness parameters are not systematical. They demonstrated that two parameters ( $S_a$  and  $S_p$ ) were necessary to characterize the studied wear phenomenon with a third body (third body interactions on peaks erosion).

Consequently, a multi-scale analysis of the  $S_a$  roughness parameter is used to characterize wear of hot rolling mill cylinders.

#### 3.3.1. Analysis of initial ground cylinder

The diagram in Fig. 6.1 represents the  $S_a$  parameter according to the high-pass Gaussian filter cut-off in a log-log scale of working cylinders at 0 km (cut-off between 1000  $\mu\text{m}$  and 4  $\mu\text{m}$ ). This diagram shows that  $S_a$  is the same all along the initial ground cylinder and for all generatrix. This indicates that the initial ground cylinder surface is homogeneous (0 km). On the same diagram, a linear trend of  $S_a$  (in log-log coordinates) according to the cut-off is observed between 1000  $\mu\text{m}$  and 17  $\mu\text{m}$ . From 17  $\mu\text{m}$  to 1000  $\mu\text{m}$ , the  $S_a$  slope is equal to  $H_1=0.4$ , leading to a fractal dimension of

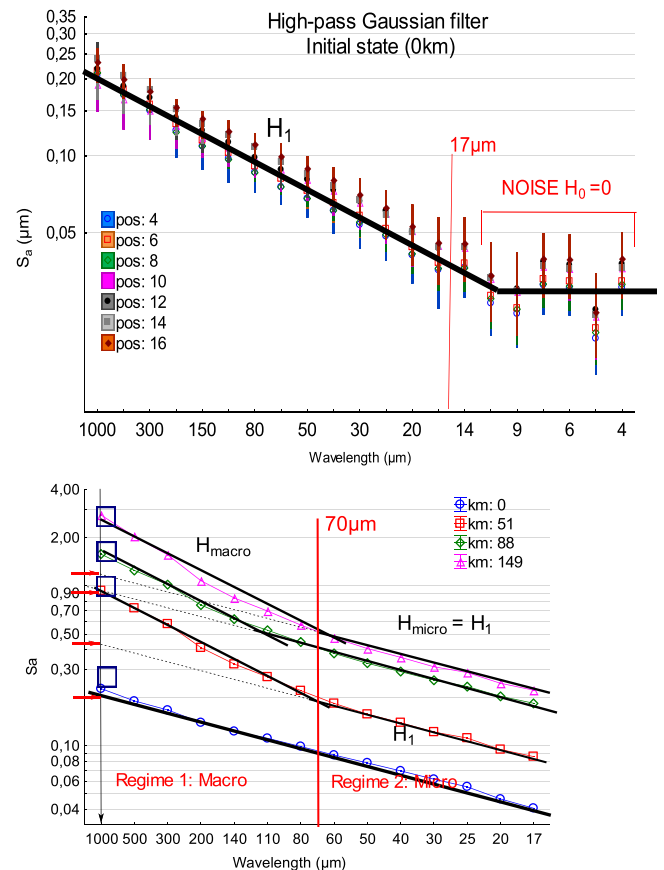


Fig. 6.  $S_a$  multi-scale evolution according to the wavelength of the high-pass Gaussian filter. (6.1)  $S_a$  multi-scale evolution of the initial ground cylinder (0 km) according to the wavelength (between 1000  $\mu\text{m}$  and 4.5  $\mu\text{m}$ ) of the high-pass Gaussian filter. (6.2)  $S_a$  multi-scale evolution of the cylinder at each kilometers (0 km, 51 km, 88 km, 149 km) according to wavelength (between 1000  $\mu\text{m}$  and 16  $\mu\text{m}$ ) of the high-pass Gaussian filter. (For interpretation of the references to color in this figure, the reader is referred to the web version of this article.)

the surface topography  $\Delta_1 = 3 - H_1 = 2.6$ . This clearly means that the grinding process leads to fractal morphology. To sum up,  $\Delta_1$  is a fractal dimension of ground surfaces.

Under  $17 \mu\text{m}$ ,  $H$  (Hurst exponent) is equal to 0, proving that the grinding process of cylinders failed to be characterized ( $H=0$  induces that surface topography can be seen as a noise whatever the scale representing a pure uncorrelated fractal process).

Physically, it means that under this critical length, surface replication by the elastomer fails to reproduce the roughness of the surface.

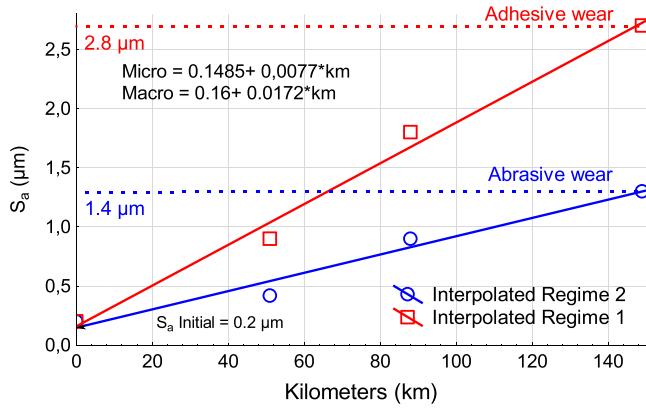
### 3.3.2. Worn cylinders

Fig. 6.2 corresponds to the same graph described in the last paragraph (Section 3.3.1), for cylinders that have rolled 0, 51, 88

**Table 3**  
Visualization of adhesion and abrasion wear according to filtering cut-off at different kilometers.

HP Gaussian filter cut-off value ( $\mu\text{m}$ )	Kilometers (km)				
	0	51	88	149	
1000					Adhesion
200					
83					
32					Abrasion
21					
17					
	Abrasion				





**Fig. 7.** Asymptotic value of  $S_a$  roughness parameter for both worn and unworn surfaces according to kilometers at full scale (1000  $\mu\text{m}$ ).

and 149 km. As shown in 3.3.1, replication of surface at 17  $\mu\text{m}$  fails. Then, our fractal analysis will be limited at a wavelength range between 17  $\mu\text{m}$  to 1000  $\mu\text{m}$ . Between 17  $\mu\text{m}$  and 1000  $\mu\text{m}$ , slopes lead to the fractal dimension of  $S_a$  at different mileages, at all locations and for every evaluation length (Fig. 6.2).  $S_a$  roughness parameter increases with the rising mileage. This is confirmed at all evaluation lengths, which means that wear exists at all evaluation lengths. All curves described in Fig. 6.2 can be split into two categories: the initial ground cylinder without wear and the 3 stages worn cylinders (51, 88, 149 km).

For the first one (0 km), the curve exhibits a power law for all the ranges of the total window length with a fractal dimension equal to  $\Delta_1=2.6$  and a Hurst exponent  $H_1=0.4$  (Hurst exponent at 0 km).

For the second set of curves corresponding to worn cylinders (51, 88, 149 km), each curve is composed of two linear parts in log-log coordinates (called bi-plot) with a threshold located around 70  $\mu\text{m}$ . In the fractal concept, this bi-plot clearly means that two different multi-scale processes exist in the cylinder damaging process: a macroscopic one over the critical length of 70  $\mu\text{m}$  and a microscopic one below 70  $\mu\text{m}$ . Then, local fractal dimension can be computed from the 3 bi-plots: macroscopic Hurst exponent  $H_{\text{macro}}$  (over 70  $\mu\text{m}$ ) and microscopic Hurst exponent  $H_{\text{micro}}$  (below 70  $\mu\text{m}$ ). From statistical analysis, it can be shown that:

- I.  $H_{\text{macro}}$  is equal to 0.6 for the 3 worn cylinders,
- II.  $H_{\text{micro}}$  is equal to 0.4 for the 3 worn cylinders,
- III.  $H_{\text{micro}}=H_{\text{macro}}=0.4$  is equal to  $H_1$  (Hurst exponent of the initial ground cylinder).

As  $H_{\text{micro}}=H_1$ , it means that both macro of worn surfaces and unworn ground cylinder have the same power law (same exponent power law). This equality of Hurst exponent and consequently of fractal dimension means that the damaging process follows the same mathematical structure describing grinding process due to abrasion. It can then be stated that, below 70  $\mu\text{m}$ , worn cylinder damage is also due to an abrasive process. Over 70  $\mu\text{m}$ ,  $H_{\text{macro}}$  increases meaning that another tribological system causes the cylinder damage that corresponds to an adhesive wear process (see Section 4). Both damaging processes can be observed in Table 3. This table describes the surfaces of the working cylinders, filtered with a high-pass Gaussian filter, at different cut-offs according to kilometers. At 0 km, only grooves from abrasion wear process are observed at all scales. From 51 km to 149 km plateaus from adhesion wear can be clearly distinguished at a cut-off between 1000  $\mu\text{m}$  and 83  $\mu\text{m}$  and grooves from abrasion wear can be clearly distinguished for a cut-off at 32  $\mu\text{m}$  and 17  $\mu\text{m}$ .

A question of major interest consists in quantifying the abrasive wear intensity and the supposed adhesive one. We have clearly

shown that the topographic amplitude is fractal and thus, whatever the wear state. Therefore there is no way to quantify wear by this topography if the latter is computed at different scales. Subsequently we decided to interpolate at macroscopic scale (1000  $\mu\text{m}$ ) the microscopic wear of the abrasive process below 70  $\mu\text{m}$ . On Fig. 6.2, the blue square symbol represents the macroscopic amplitude of roughness and the red filled arrow symbol represents the interpolated micro-roughness amplitude at the macroscale if no adhesive wear occurs.

The interpolated values from microscopical and macroscopical amplitude are plotted according to kilometers of cylinders (Fig. 7). The  $S_a$  parameter linearly increases for both regimes with the mileage of cylinders but slope is twice higher for interpolated regime no. 1 (adhesive wear) than for interpolated regime no. 2 (abrasive wear). It clearly means that adhesive processes are twice more intense than abrasive processes.

### 3.3.3. Radial, axial and vertical morphology's homogeneity

As already discussed in our statistical analysis, Fig. 5 reveals that "radial effect" can be neglected compared to the mileage, vertical position of working cylinders and axial position of replicas. This implies that wear is homogeneous on the full circumference of the cylinder and, in terms of process conditions, no circularity errors are introduced during the grinding process. Statistical analysis of variance leads to the following results:

1. It can be statistically proved that the roughness of inferior and superior cylinders for the initial ground cylinder (0 km) is similar with a high confidence level. Consequently, future differences between the inferior and superior cylinder morphologies cannot be due to the difference of the initial roughness state.
2. For intermediate worn cylinder (51 and 88 km), the  $S_a$  curves (Fig. 8) present a U-shape for the superior cylinder and a W-shape for the inferior cylinder. This means that, for superior cylinder, wear is maintained at locations 4 and 16. These points correspond to the contact border between the cylinder and the edges of steel sheet. It can be explained by several phenomena occurring in the same section of the cylinder's surface. Indeed, flexion of rolls during rolling implies a maximal stress on this section. Moreover, a thermal effect is suspected because the steel strip is colder in this section of the cylinder's surface leading to a higher hardness of the product that could increase damage intensity during rolling.

On the inferior cylinder after 51 and 88 km rolling, W-shape of  $S_a$  curves means that wear is quite the same in the center of the steel sheet than on the edges. Here, we can suppose that the increase in surface roughness could be due to thermal crown of the roll that will imply a higher stress on product surface. As a result, wear will be promoted by thermal crown in the middle of the cylinder and by colder product edges in cylinder extremities.

For the most worn surface (at 149 km) we have an interesting inverted U-shape of  $S_a$  curves. It can be the result of an extended consequence of thermal crown that propagates along the cylinder width. When thermal crown is so high that wear is impacted along its whole length, it means that the cylinder is out of order. This surface assessment method can be used as a testing method to evaluate cylinder surface quality and it could define a criterion to optimize grinding operations frequency.

## 4. Interpretations

Stripes are detected (Fig. 9) on worn hot rolling mill cylinders and are due to transfer bar abrasion that occurs during rolling in

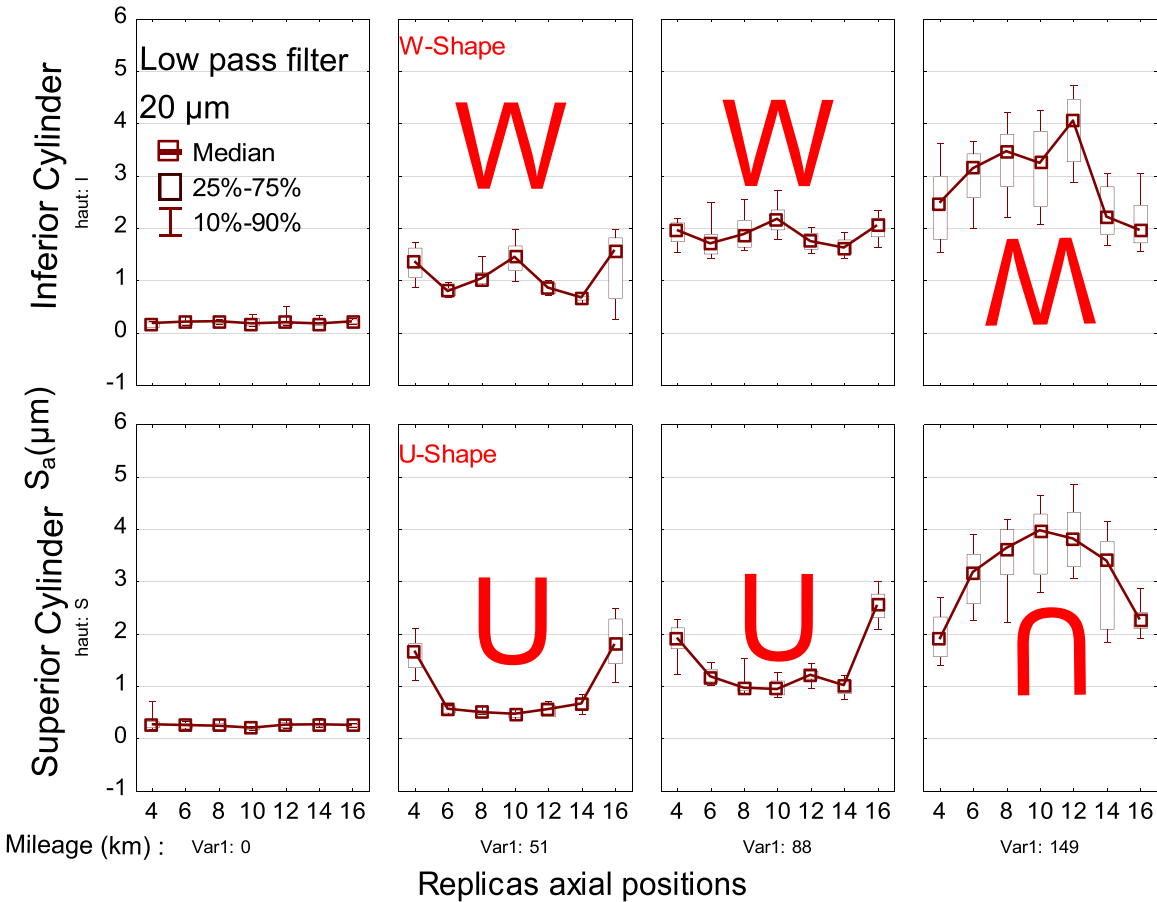


Fig. 8.  $S_a$  parameter's evolution according the vertical position of working cylinder and the axial replica location at each different mileages.

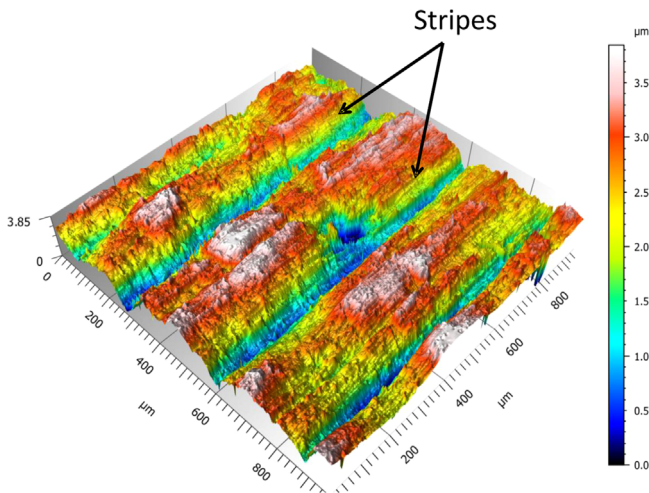


Fig. 9. Hot rolling mill stripes description.

finishing stands. Stripes are oriented along rolling direction which is characteristic of HSS (High Speed Steels) roll wear [4,14,16], because of its high oxidation resistance at high temperatures.

On the studies related to ferritic stainless steels, grooves located in between the stripes were identified as the main cause of a surface defect initiation called « rolled-in-scale » by Jin et al. [4]. The depth of grooves is the main criterion related to defect severity [4,14]. If the groove is deeper than the transfer bar oxide layer, the defect will be initiated [14]. It results in a sticking of one transfer bar particle containing oxide and ductile stainless steel

base metal onto the cylinder surface inside the groove. This first mechanism corresponds to the abrasive wear process (Fig. 10) also detected as the interpolated regime no. 2 on the previous figure (Fig. 7). Then, this particle is a nucleation site for the sticking phenomenon that will be reproduced at each cylinder rotation (Fig. 10), leading to a macroscopic defect on stainless steel surface when the grown particle is transferred back to the product after reaching a critical size. This second phenomenon corresponds to the adhesive wear process (Fig. 10) also detected as the interpolated regime no. 1 on the previous figure (Fig. 7).

Afferrante et al. [19] showed on simulated rough surfaces (using the Weierstrass function) that in a full contact at small scales of roughness, adhesion wear cannot occur for fractal dimensions greater than 2.5. For a partial contact, when the fractal dimension  $D$  is superior to 1.5, the adhesion does not affect the contact behavior. At the opposite, when the fractal dimension is less than 1.5, complete contact occurs at small scale. This totally agrees with the adhesive wear mechanism (Regime 1, Fig. 6.2) initiated by small scratch caused by abrasive wear. The oxide aggregate will nucleate on the scratch of mean size “ $d$ ” inferior to “ $s$ ” ( $s$ : size of final oxide aggregate when the grown particle is transferred back to the product). It lets us to think that the threshold of the bi-plot curves is equal to this critical size. Under this size, adhesion cannot occur because the fractal dimension of surface is greater than 2.5. Then over  $70 \mu\text{m}$ , adhesion can occur because the fractal dimension is inferior to 2.5 and according to Johnson, Kendall and Roberts (JKR) theory on fractal surfaces, the contact will be full (adhesion oxide-product) leading to adhesive wear.

On industrial statistics, it was clearly highlighted that sticking defect intensity increases with cylinder wear. There is a first order

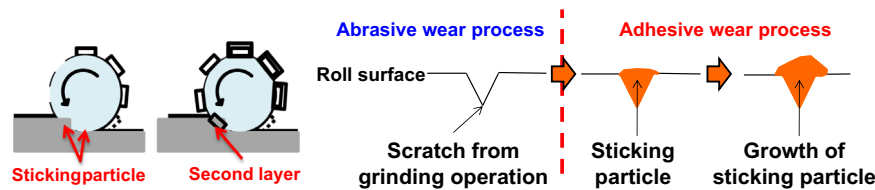


Fig. 10. Defect initiation mechanism of working cylinders during hot rolling mill process.

dependence between the defect initiation and the number of cylinder rolled kilometers. Therefore the campaign length was limited to avoid the defect but it implies an increasing number of grinding operations and cylinders change onto the production lines on some particular products.

## 5. Conclusion

To sum up, the targets of this study were:

- to find a non-destructive method, compatible with industrial context, to analyze roll surface wear and roughness,
- to define a criterion that will determine the maximal length of rolling campaigns before grinding,
- to highlight the main industrial actuators that have a strong impact on roll wear (towards this sticking phenomenon).

The working roll replicas analyzed with interferometer show a high reproducibility of the surface aspect when roughness is analyzed over 16  $\mu\text{m}$  wavelength. It allows confirming that rolled kilometers were a first order of importance in cylinder damage, matching to the industrial findings conducted on defect investigations.

By the  $S_a$  parameter evolution analyses along cylinder width, it was noticed that the trend can have different shapes (U, W or  $\cap$ ).

U-shape is characteristic of a low wear (reduced number of rolled kilometers) and reveals that colder product edges induce particular cylinder damage.

W-shape is characteristic of a medium wear; it means that, as soon as we will notice this trend on the cylinder, it is able to run more kilometers; a grinding operation is not still necessary.

The  $\cap$ -shape is characteristic of a high wear meaning that the cylinders have to be ground in order to prevent from severe sticking phenomenon.

This criterion will help us extend the time between two successive grinding operations, optimize other rolling process parameters and also increase the length of hot rolling campaigns.

## References

- [1] Luc E, Bigerelle M, Deltombe R, Dubar M. The representative topography of worn hot rolling mill cylinders. *Tribol Int* 2015;82:387–99. <http://dx.doi.org/10.1016/j.triboint.2014.05.031>.

- [2] Lee S, Jin W, Suh D, Oh S. Sticking mechanism during hot rolling of two stainless steels. *Metall Mater Trans A* 1998;29(February):696–702. <http://dx.doi.org/10.1007/s11661-998-0151-9>.
- [3] Won J, Choi J-Y, Yun-Yong L. Effect of roll and rolling temperatures on sticking behavior of ferritic stainless steels. *ISIJ Int* 1998;38(7):739–43. <http://dx.doi.org/10.2355/isijinternational.38.739>.
- [4] Won J, Choi J-Y, Yun-Yong L. Nucleation and growth process of sticking particles in ferritic stainless steel. *ISIJ Int* 2000;40(8):789–93. <http://dx.doi.org/10.2355/isijinternational.40.789>.
- [5] Ha DJ, Sung HK, Lee S, Lee JS, Lee YD. Analysis and prevention of sticking occurring during hot rolling of ferritic stainless steel. *Mater Sci Eng: A* 2009;507(1–2):66–73. <http://dx.doi.org/10.1016/j.msea.2008.11.062>.
- [6] Deltombe R, Kubiak KJ, Bigerelle M. How to select the most relevant 3D roughness parameters of a surface. *Scanning* 2014;36:150–60. <http://dx.doi.org/10.1002/sca.21113>.
- [7] Bigerelle M, Najjar D, Mathia T, Iost A, Coorevits T, Anselme K. An expert system to characterise the surfaces morphological properties according to their tribological functionalities: the relevance of a pair of roughness parameters. *Tribol Int* 2013;59:190–202. <http://dx.doi.org/10.1016/j.triboint.2012.04.027>.
- [8] ISO 16610-21. Geometrical Product Specifications (GPS) – Filtration – Part 21: Linear profile filters: Gaussian filters; 2011.
- [9] ASME B46.1. Surface texture: surface roughness waviness, and lay, New York: American Society of Mechanical Engineers; 2009.
- [10] ISO 25178-2. Geometrical product specifications (GPS)-Surface texture: Areal - Part 2: Terms, definitions and surface texture parameters, 2012.
- [11] Stout K, Sullivan P, Dong W, Mainsah E, Luo N, Mathia T, et al. The development of methods for the characterisation of roughness in three dimensions. Commission of the European Communities; 1993 EUR 15178N.
- [12] Tehrani M, Malbrancke J, Vergne C. Work rolls in the roughing mills: roll grade and process optimization to save energy and roll cost of use (winrolls). Commission of the European Communities; 2014 EUR 26421 EN.
- [13] Prado M, Lima LC, Simão R a. Scale laws for AFM image evaluation : potentialities and applications. *Curr Microsc Contrib Adv Sci Technol* 2012:923–9.
- [14] Luc E. Initiation of sticking phenomenon in hot roll ing of ferritic stainless steels. *Sciences Pour l'Ingénieur (SPI)*; 2013.
- [15] Najjar D, Bigerelle M, Iost A. The computer-based bootstrap method as a tool to select a relevant surface roughness parameter. *Wear* 2003;254:450–60. [http://dx.doi.org/10.1016/S0043-1648\(03\)00140-6](http://dx.doi.org/10.1016/S0043-1648(03)00140-6).
- [16] Guillot I. Oxydation et phénomènes de frottement à chaud sur les aciers inoxydables ferritiques: influence des elements mineurs (Ti, Nb, Mo). Université Technologique de Compiègne; 1990.
- [17] De Chiffre L, Lonardo P, Trumpold H, Lucca DA, Goch G, Brown CA, et al. Quantitative characterisation of surface texture. *CIRP Ann Manuf Technol* 2000;49(2):635–52.
- [18] Berglund J, Agunwamba C, Powers B, Brown C, Rosén B-G. On discovering relevant scales in surface roughness measurement – an evaluation of a band-pass method. *Scanning* 2010;32(4):244–9.
- [19] Afferrante L, Ciavarella M, Demelio G. Adhesive contact of the Weierstrass profile. *Proc R Soc A* 2015;471(2182):20150248.